



## Study on the properties of a nanofiltration membrane with O-MoS<sub>2</sub> nano-composite substrate and the applications in dye wastewater treatment

Yiwen Wang<sup>a,b</sup>, Qinliang Jiang<sup>a,c,\*</sup>, Hua Fan<sup>b</sup>, Lihe Wang<sup>a</sup>, Jihai Xiong<sup>a</sup>, Jianquan Luo<sup>c</sup>

<sup>a</sup>Institute of Energy Research, Jiangxi Academy of Sciences, Nanchang 330096, China, email: qljiangxas@163.com

<sup>b</sup>Key Laboratory of Poyang Lake Environment and Resource Utilization, Ministry of Education, School of Resources Environmental and Chemical Engineering, Nanchang University, Nanchang 330031, China

<sup>c</sup>University of Chinese Academy of Sciences, Institute of Process Engineering, Chinese Academy of Sciences, State Key Laboratory of Biochemical Engineering, School of Chemical Engineering, Beijing 100049, Peoples R China

Received 24 February 2022; Accepted 21 August 2022

### ABSTRACT

A novel thin-film nanofiltration (NF) membrane was prepared successfully by interfacial polymerization of piperazine and trimesoyl chloride on a porous molybdenum disulfide oxide (O-MoS<sub>2</sub>) modified polysulfone (PSf) substrate with greatly enhanced separation performance. In this work, scanning electron microscopy confirmed that the optimized PSf substrate formed elongated finger-like pores during the phase inversion process, significantly different from other membranes and key to improving the water transport and desalination of the membrane. The effects of different dye molecular structures, varieties, and charges, and the feed solution and salt concentrations in the blend solution on salt and dye rejection and water flux of NF membranes were explored. Compared with the control membrane, the optimized membrane's rejection performance and water permeability were greatly improved when treating simulated dye wastewater. After the introduction of O-MoS<sub>2</sub> (0.06 wt.%), the introduction of O-MoS<sub>2</sub> increased the chromotropic acid 2B and Rose Bengal rejection rates of the membrane compared to the original, from the original of 97.73%, 99.79% to 99.41% and 99.99%, respectively, and the water flux enhanced from the beginning of 32.8, 32.0–43.2 and 43.7 L/m<sup>2</sup>-h, respectively. Furthermore, in a 120 h simulated dye wastewater treatment stability test, the optimized F6 membrane showed stronger flux stability and excellent rejection performance, providing its vast potential for application in dye wastewater treatment.

*Keywords:* Nanocomposite substrate; Nanofiltration membrane; Molybdenum disulfide oxide (O-MoS<sub>2</sub>); Dye wastewater; Treatment

### 1. Introduction

The textile industry is one of the most important economic sources for many countries. In China, textile products account for 13%–15% of China's total exports and 5%–6% of China's total gross domestic product, also high-polluting sources [1–4]. According to the China Environmental Yearbook statistics, the textile industry ranks third in the discharge of industrial wastewater in various industries. In addition to the colored dye molecules in textile printing

and dyeing wastewater, many inorganic salts are produced by the neutralization reaction and salting-out process (salt-induced precipitation) of dye synthesis and concentration. Simultaneously, some slats are used as additives to improve absorption during the dyeing process [5]. The direct discharge of these organic dyes and salts into the water causes serious environmental problems. Therefore, finding a suitable treatment method for textile printing and dyeing wastewater is very important.

\* Corresponding author.

Traditional wastewater treatment processes, such as advanced oxidation, adsorption, and biological methods, have disadvantages. For example, the advanced oxidation method will cause a large amount of sludge, produce secondary pollution, and require sophisticated equipment. In conventional physical methods, such as adsorption and extraction, the regeneration cost of adsorbent and extractant is very high, and it is easy to cause secondary pollution to water resources. The main disadvantage of biological methods is that external factors such as pH value and dye concentration greatly affect microorganisms and are difficult to control. Hence, membrane technology has emerged as a relatively low-cost, environmentally sustainable, and energy-efficient pollution control and treatment method [6–8]. Membrane technology to treat dye wastewater can avoid secondary pollution, has high reliability, and is easy to operate, overcoming some of the shortcomings of traditional wastewater treatment processes [9,10]. At the same time, within the framework of sustainable development, membrane technology can remove pollutants from water and recover dye molecules and salts, making textile wastewater a potential resource.

Nanofiltration is a very complex process. Current studies have shown that electrostatic interaction (Donnan Effect) and steric hindrance dominate the membrane retention and permeation performance in the nanofiltration process [11]. The membrane's pore size and the charge of the contaminants (dyes and salts) affect their performance [12]. Since the steric hindrance effect dominates the filtration process, controlling the membrane's pore size by adding well-defined two-dimensional (2D) nanomaterials to provide additional nanochannels is an excellent way to improve membrane performance and enhance membrane selectivity [13–17]. Experiments have shown that changes in the base film's properties will affect the film's rejection behavior [18–21]. Hence, we considered the incorporation of modified 2D nanomaterials into the membrane matrix to modulate the membrane properties. In addition, due to the electrostatic effect, a surface-charged membrane tends to help nanofiltration (NF) membranes to perform better dye/salt separation and rejection, with better permeation performance and contamination resistance, especially for some low molecular weight dyestuff molecules [22]. The membrane surface charge of this base-membrane modified nanofiltration membrane is also changed by the modified nanoparticles, improving the filtration performance of the membrane [23].

This study used a laboratory-made molybdenum disulfide oxide (O-MoS<sub>2</sub>) modified base-NF membrane to filter simulated dye wastewater. We conducted a preliminary study on the application of modified NF membranes in dye wastewater. The simulated dye wastewater composition examination after filtering showed that the filtration performance of the O-MoS<sub>2</sub> modified base-NF membrane was superior to the control membrane. More importantly, the membrane performance change pattern was investigated by changing the composition of the simulated wastewater, and the general application range of this modified NF base membrane was also obtained. In addition, the potential application of the prepared NF membrane was demonstrated by the long-term separation of simulated dye wastewater. The membrane was evaluated for its separation efficiency and

stability against salts and dyes under long-term operating conditions. This work showed that nanofiltration membranes prepared by modifying the membranes' matrix with nanomaterials performed better in separating and recovering dye wastewater. The prepared NF membrane with more straightforward fabrication procedures and reproducible results has more substantial advantages and application prospects in dye removal.

## 2. Experiment

### 2.1. Materials

The modified membranes prepared in the laboratory are named after the concentration of O-MoS<sub>2</sub> added to the membranes, respectively F0, F3 (0.03 wt.% O-MoS<sub>2</sub>), F6 (0.06 wt.% O-MoS<sub>2</sub>), F9 (0.09 wt.% O-MoS<sub>2</sub>) and F12 (0.12 wt.% O-MoS<sub>2</sub>). Used to test the separation performance of inorganic salts Na<sub>2</sub>SO<sub>4</sub> (99%), NaCl (99.5%), dye Rose Bengal (95%), chromotropic acid 2B (97%), lemon yellow (>95% high-performance liquid chromatography (HPLC)), Jiana Green B (dye content 65%), all purchased from Aladdin (Shanghai). The experimental water is self-made in the laboratory (deionized water and ultra-pure water).

### 2.2. Characterization and testing of the NF membranes performance

The O-MoS<sub>2</sub> nanoparticles were added to the casting solution at different proportions. They were uniformly dispersed into the membrane matrix for 2 h with ultrasonic vibration and 12 h with mechanical stirring. The NF membrane substrate was prepared by dry-wet separation phase inversion. Then, on the surface of the base film, a selective layer was prepared by interfacial polymerization. An aqueous solution of 1.50 wt.% (±)-camphor-10-sulfonic acid (99%, Aladdin), 1.50 wt.% triethylamine (99%, Aladdin) and 1.60 wt.% piperazine (99%, Aladdin) was selected as the water phase and the base film was immersed for 35 s. After draining the aqueous solution, the membrane surface was allowed to dry again. Next, an *n*-hexane solution containing 0.35 wt.%/v% of 1,3,5-benzenetricarbonyl trichloride (98%, Aladdin) was selected as the oil phase, followed by immersing in the membrane for 20 s. The oil phase solution was drained from the surface of the membrane, and the membrane was dried in an oven at 60°C for 2 min to obtain the NF membrane required for the experiment.

The slices were extracted with liquid nitrogen before sample preparation, and gold was sprayed with Hitachi E-1010 gold sprayer before the test (Hitachi, Japan). Scanning electron microscopy (SEM, S3400N, Hitachi, Japan) and transmission electron microscopy (TEM, H-7650, Hitachi, Japan) were used to examine the basic morphological features of NF membranes. The membrane matrix was also tested for hydrophilicity and presented in the form of water contact angle (OCA15EC, DataPhysics, Germany) by dropping 2 μL deionized water onto the membrane surface. Test the ionic conductivity of the solution to be determined using a conductivity meter (DDS-307A, Shanghai Lei Magnetic Instrument Factory, China). Simultaneous determination of the dye influent and effluent concentration was tested

with an ultraviolet-visible analyzer (UV-1800, Shimadzu Corporation, Japan).

### 2.3. Membrane application test

To explore the application ability of the laboratory-made membrane in the treatment of dye wastewater, a variety of simulation tests were carried out on it.

A cup-type NF test system was used, and the membrane was preloaded at 0.5 MPa for 0.5 h, and then the pure water flux  $J_w$  of the membrane was measured at 0.4 MPa. The pure water flux is calculated according to Eq. (1):

$$J_w = \frac{V}{At} \quad (1)$$

where  $J_w$  is the pure water flux of the membrane, L/m<sup>2</sup>·h;  $V$  is the product water volume, L;  $A$  is the effective membrane area, m<sup>2</sup>;  $t$  is the filtration time, h.

The rejection rate of the membrane is calculated according to Eq. (2):

$$R = \left( 1 - \frac{C_p}{C_f} \right) \times 100\% \quad (2)$$

where  $R$  is the solute rejection rate, %;  $C_p$  is the product water concentration, g/L;  $C_f$  is the influent water concentration, g/L.

## 3. Results and discussion

### 3.1. Properties of the modified of the experimental self-made NF membrane

Membrane materials dominate the membrane separation properties. The performance of the membrane material determines the separation selectivity, water permeability, pollution resistance, acid and alkali resistance, and oxidation resistance of the membrane in the separation process [24]. To meet dye wastewater treatment requirements,

improve the efficiency of the NF process, enhance the NF membrane water permeability, selectivity, and durability, and simultaneously reduce water flux loss, we added O-MoS<sub>2</sub>, a 2D nanomaterial, to the NF membrane support layer. Then the polyamide (PA) layer of interface polymerization was loaded on the support layer. On the one hand, we expected the electronegativity of O-MoS<sub>2</sub> can make an make the NF film surface electronegative [25], strengthening the electrostatic repulsion during interception, and improving the membrane's interception performance. In addition, the O-MoS<sub>2</sub> water affinity can improve the hydrophilicity of membrane substrates and affect the phase inversion process of the NF membrane support layer, while further influencing the interfacial polymerization of the produced membrane selective layer [26]. Furthermore, the lamellar structure of 2D nanomaterials can increase the water channels additionally for membrane substrate, which can also increase the water flux of the membrane [27].

As shown in the TEM images (Fig. S1), the PA layer firmly loaded on the F0 and F6 membranes improved NF membrane selectivity effectively. Moreover, the O-MoS<sub>2</sub> nanoparticles are embedded in the modified membrane substrate. Compared with the control membrane F0, the 2D nanoparticles that changed the physico-chemical properties of the substrate are the key to the membrane's performance improvement [28]. The cross-sectional SEM images of the NF membrane are shown in Fig. 2a1–a5. When the O-MoS<sub>2</sub> content in the membrane reaches 0.06 wt.%, the structure and morphology of the composite membrane change greatly. The 2D nanomaterials greatly impact the phase inversion process. Compared with the control membrane F0, the F6 membrane formed elongated finger-like pores during the phase inversion process of dry and wet separation. The slender finger-like holes improve water conservancy when water passes through the membrane, which is more conducive to water transportation and salt rejection [18]. The initial formation of the wide asymmetrical holes made the tunnel even more tortuous [29]. As the highly hydrophilic O-MoS<sub>2</sub> content increases, the cast film solution becomes more hydrophilic and the increase of the cast film solution viscosity (Table S1) leads to the secondary phase transformation of the membrane. The slender finger-like pores shrunk, and became thicker and shorter, forming the undesired membrane pore structure that will reduce the water flux of the membrane, while the increase in membrane pore size will also hinder salt retention. Fig. 2b1–b5 show the SEM images of the NF membrane surfaces. Under the same magnification, clear visible bubble-like protrusions, typical morphology of interfacial polymerization, are visible [30,31]. Compared with the control film F0 of Fig. 2b1, take the best-performing membrane F6 of Fig. 2b3 as an example, the F6 membrane surface with more small bubble-like bumps looked rougher than F0. The increase in roughness may also cause an increase in membrane water flux [32]. This is due to increased hydrophilicity of the substrate membrane and more complete interfacial polymerization reaction on the membrane surface. This is also evidenced by the atomic force microscopy (AFM) surface roughness tests (Fig. S2 and Table S2) performed on the surface of the NF membrane.

To determine the effect of nanoparticles on the surface properties of the membrane substrate, the hydrophilic

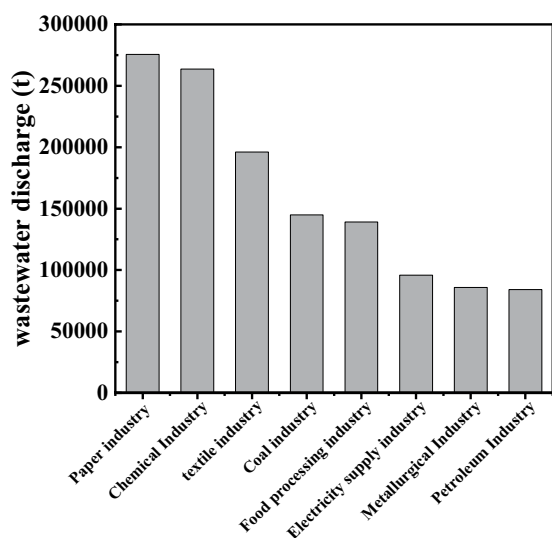


Fig. 1. China's wastewater emissions by industry.

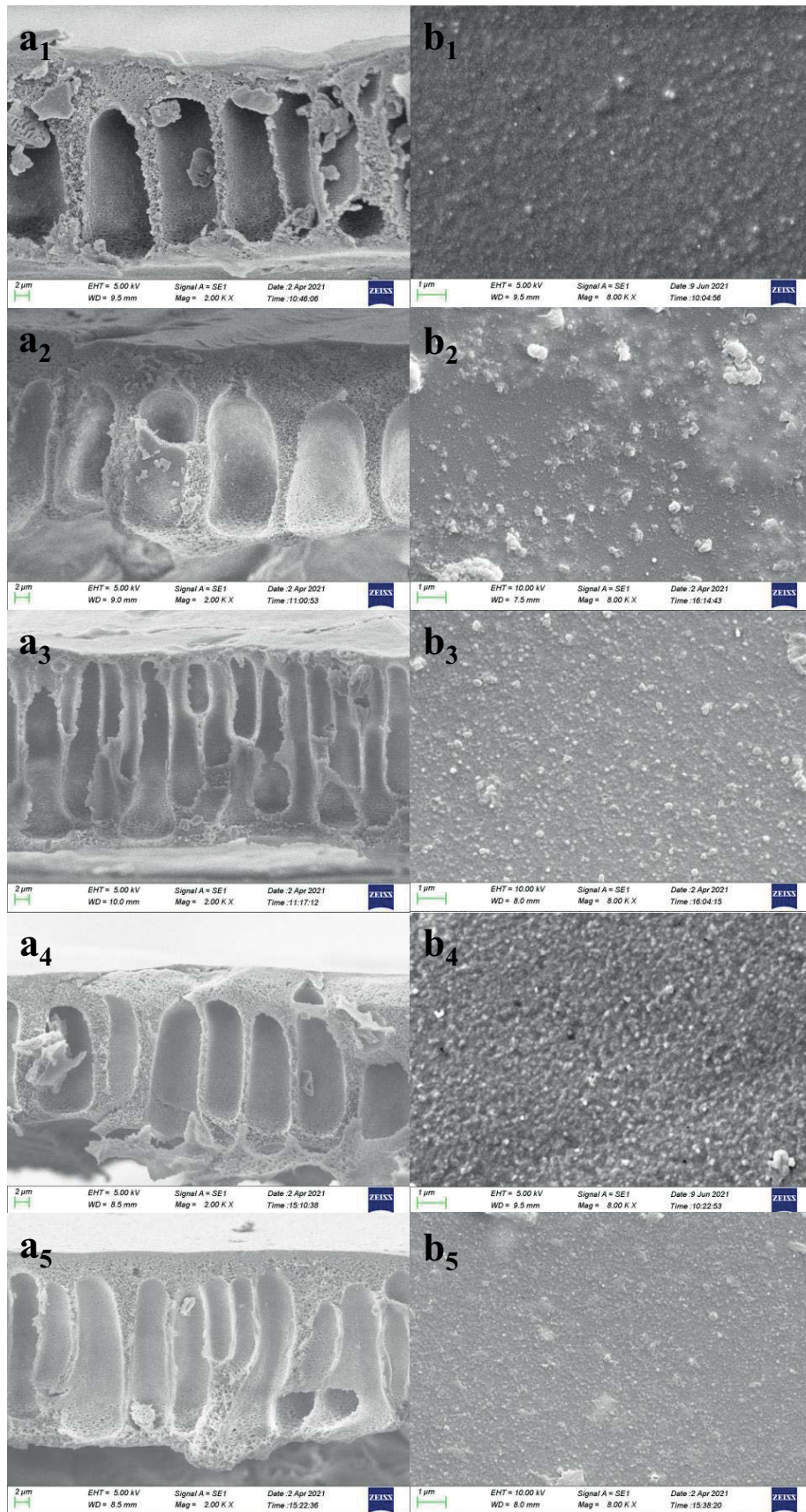


Fig. 2. SEM images of the cross-sectional (a1–a5) and surface (b1–b5) morphologies of the NF membranes (F0, F3, F6, F9 and F12).



properties of the substrate surface were tested for water contact angle. The experimental results are shown in Table 1. Incorporating hydrophilic O-MoS<sub>2</sub> greatly improved the hydrophilicity of the substrate film surface, and the hydrophilicity increased with nanoparticle content.

The separation and permeation performances of membranes are essential for evaluating membranes. Fig. 3 shows the water flux test (a) and the salt rejection test (b) result represented by Na<sub>2</sub>SO<sub>4</sub>. Adding an appropriate amount of O-MoS<sub>2</sub> effectively increased the water flux of the membrane from 36.8 L/m<sup>2</sup>·h at F0 to 64.8 L/m<sup>2</sup>·h at F6, and the membrane water flux increased by about 76%. This was mainly because the added O-MoS<sub>2</sub> improved the hydrophilicity of the modified membrane to a certain extent and increased the roughness of the membrane surface. At the same time, O-MoS<sub>2</sub> provided extra water channels in the membrane matrix [33]. Also, phase inversion was affected due to the viscosity and hydrophilicity changes in the casting solution. Long and straight membrane pores were formed throughout the membrane, shortening the transport time of water molecules in the irregular spongy pores and reducing the resistance of water molecule transfer. The large cavity of the membrane substrate layer and the long and straight pore structure reduced the resistance when water molecules passed through the membrane, speeding up the transmission rate of water molecules, and increasing the membrane's permeability [34]. In addition, due to the hydrophilicity increase of the membrane matrix, the cross-linking degree of the selective PA layer on the NF membrane surface was also increased. The defect-free selective layer has better hydrophilicity; the water molecules pass through the membrane






more easily [26]. When the content of the 2D materials continued to increase, the flux would decrease compared with F6. This can be explained by the substrate membrane being more hydrophilic, resulting in a denser and thicker PA layer on the membrane surface, making it more difficult for water molecules to pass through the membrane [26,35,36]. In addition, O-MoS<sub>2</sub> agglomerated with the O-MoS<sub>2</sub> content increase in the membrane support layer, affecting the NF membrane performance and reducing the additional water channel supply. Therefore, the membrane water flux was reduced [37].

In Fig. 3b, the salt rejection of the O-MoS<sub>2</sub>-modified membrane was significantly improved. For the 1 g/L sodium sulfate solution, the rejection capacity of F6 and F9 reached 96.6% and 96.0%, was much higher than the 87.4% in F0. Three representative membranes, F0, F6, and F12, were selected for the membrane molecular weight cut-off (MWCO) test to better determine the reasons for the performance change. The specific test method is described in the Supporting Information. The obtained results are shown in Table 2. Concomitant with the membrane pore size change observed in the cross-sectional SEM images, the addition

Table 2  
NF membrane MWCO

Membrane no.	MWCO (Da)
F0	1,260
F6	937
F12	1,401

Table 1  
Membrane substrate water contact angle

F0	F3	F6	F9	F12
				
73.7	67.3	62.1	56.0	51.4

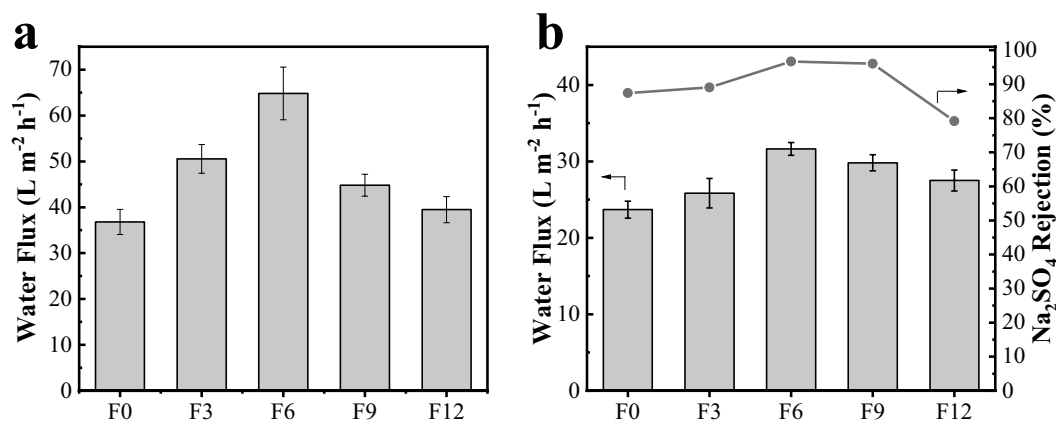


Fig. 3. Membrane basic performance test (a) pure water flux and (b) Na<sub>2</sub>SO<sub>4</sub> rejection and water flux.

of O-MoS<sub>2</sub> affected the membrane substrate, the larger the pore size of the membrane matrix, the more likely interfacial polymerization would occur in the membrane pores. The PA selective layer on the NF membrane surface is more discontinuous and defective, resulting in poorer rejection performance [38,39]. Affected by the rejection mechanism of NF membrane–steric hindrance effect, the membrane with a smaller pore size for the same salt ion will show better salt rejection capacity [40,41].

### 3.2. Membrane separation performance and application

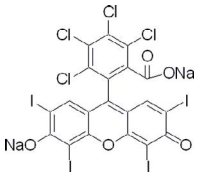
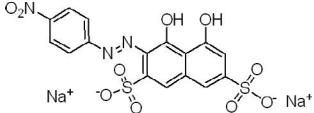
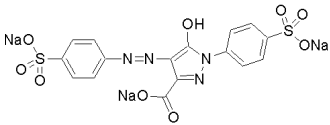
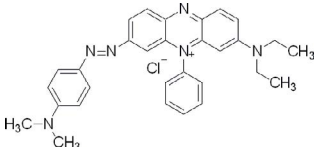
#### 3.2.1. Single dye and salt rejection performance test

Since the introduction of O-MoS<sub>2</sub> greatly impacted the structure and morphology of the composite membrane and effectively improved its properties, we further studied separation performance and rejection behavior of the composite membrane modified with different amounts of O-MoS<sub>2</sub>. Two dyes with large molecular weight differences, Rose Bengal (RB) and chromotropic acid 2B (CB), were selected; the specific information of the two dyes is shown in Table 3. A 30 mg/L pure dye aqueous solution was used for testing, and the flux and rejection performance results of single dye solutions are shown in Fig. 4a and b. The rejection and flux of the polysulfone (PSf) membrane without O-MoS<sub>2</sub> (F0) were relatively small. Rejection of CB and RB of F0 was 97.73% and 99.79%, respectively, and the flux was 32.8 and 32.0 L/m<sup>2</sup>·h. After the introduction of O-MoS<sub>2</sub>, the rejection of dyes by the composite membrane was significantly improved. Among them, the F6 membrane had the best performance, with a rejection rate of 99.41%

and 100% for the two dyes (CB and RB). The flux has also reached to 43.2 L/m<sup>2</sup>·h of CB and 43.7 L/m<sup>2</sup>·h of RB, respectively. The rejection rate and water flux were higher than those of membrane F0. Since the separation mechanism of NF membranes was mostly due to steric hindrance and sieving effect, the membrane F6 with a smaller pore size had a more significant repelling effect on the model pollutant, improving the rejection [42]. Meanwhile, because the layered structure of the hydrophilic O-MoS<sub>2</sub> provided additional water channels, the flux of the composite membrane was also larger than the control membrane F0. The O-MoS<sub>2</sub> modified base-NF membrane overcame the trade-off effect of NF membranes to a certain extent, and simultaneously improved the rejection performance and water flux.

To further explore the application of the composite membrane in the rejection of dyes, the rejection performance and water flux of the two model pollutants at different concentrations were tested, as shown in Fig. 4c–f. Fig. 4c and d, show the rejection rates of different CB and RB concentrations. The results showed that the higher the dye solution concentration, the lower the rejection rate of the membrane, which is in line with the general law of NF membranes [8]. Fig. 4c shows that the different amounts of nanomaterials affect the membrane's rejection performance. Membrane F6 and F9 exhibit better rejection effects when the solution concentration is lower; the rejection rates reached 99.41% and 99.27%, respectively, when the dye concentration is 30 mg/L. CB has a smaller molecular size than RB, and the significant change in the rejection performance can be attributed to the significant reduction in the size of the basement membrane pores. This further indicates

Table 3  
Characteristics of the small molecule dyes used in the experiment

Dye name	Molecular structure	Relative molecular mass	Charge	Ultraviolet absorption peak wavelength (nm)
Rose Bengal (RB)		1017.64	Negative	550
Chromotropic acid 2B (CB)		513.37	Negative	515
Lemon yellow (LY)		534.36	Neutral	426
Jiana Green B (JGB)		511.06	Positive	615

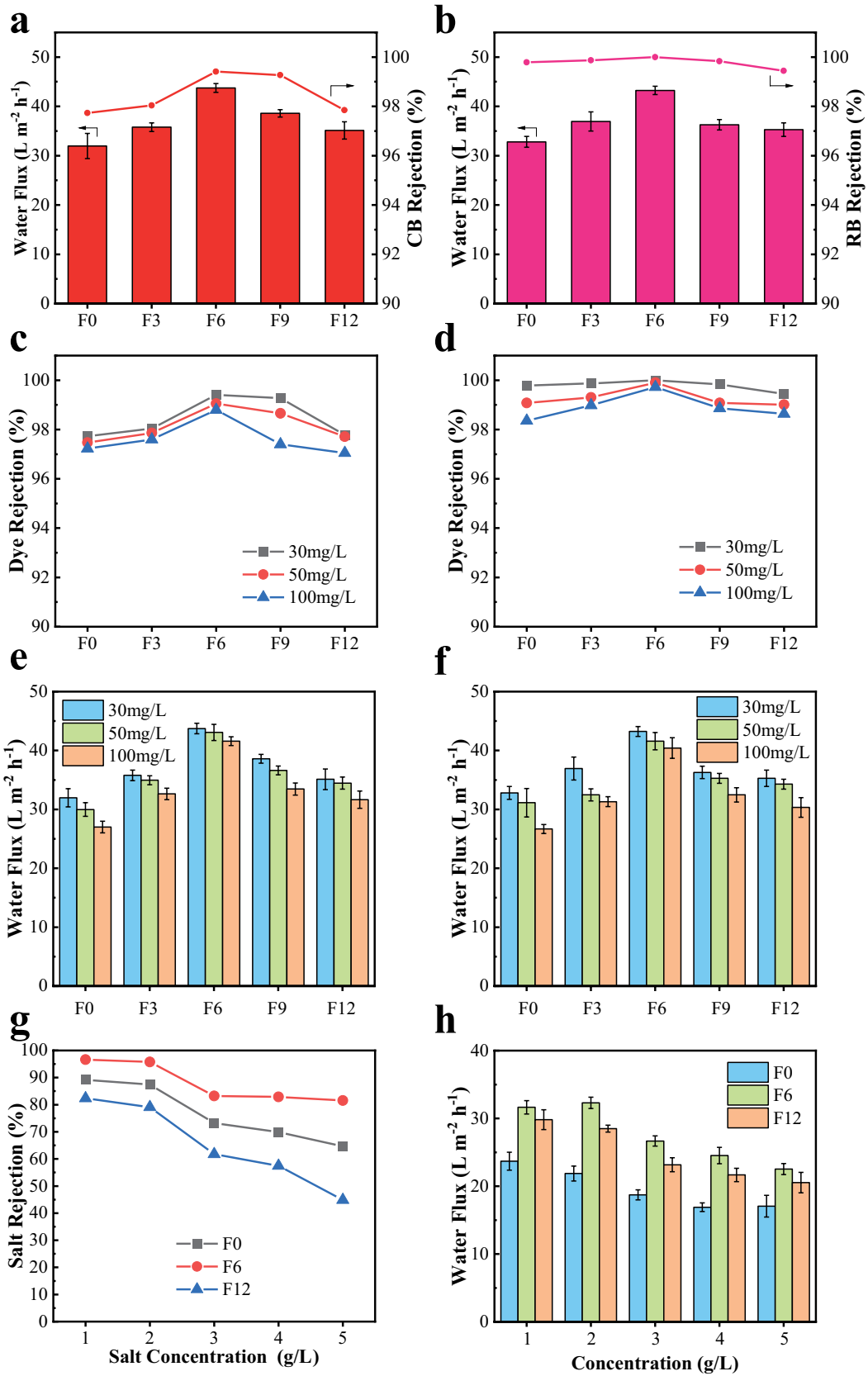


Fig. 4. Single pollutant interception and flux test (a,b) 30 mg/L CB, RB interception and flux, (c,d) different concentration of CB interception performance and flux changes, (e,f) interception performance and flux changes of different concentrations of RB, and (g,h) interruption and flux changes of different salt concentrations.

that O-MoS<sub>2</sub> in the membrane's support layer improves the pore morphology and performance of the membrane to a greater extent during the phase inversion process. The RB rejection rate change shown in Fig. 4d demonstrated the effect of dye concentration changes on the rejection rate. When the dye concentration increases, the rejection rate of the PSf membrane decreases from 99.79% at 30 mg/L to 98.36% at 100 mg/L. Due to the larger molecular size of RB, the change in rejection rate may be more dependent on the increased electrostatic effect. Since the negatively charged O-MoS<sub>2</sub> was added to the membrane matrix in an appropriate amount (0.06 wt.%), the electrical properties of the membrane surface were effectively improved, the electrostatic effect during membrane rejection was enhanced, and the rejection effect of the membrane was improved [43]. The decay of the better performing membrane F6 is smaller, from 100% at 30 mg/L to 99.72% at 100 mg/L.

Fig. 4e and f show the water flux changes of CB and RB under different concentrations, respectively. When the dye concentration increased, the water flux of each membrane decreased. This is because as the dye concentration increases, the tendency of membrane fouling and the viscosity of the dye solution increase. At the same time, due to the larger molecular weight of RB, it was easier to form a thicker "filter cake" on the surface of the membrane, preventing water molecules from passing through the membrane to a certain extent [44]. Therefore, compared with the smaller molecular weight of CB, the water flux during filtration will also become smaller. Besides, with increased dye solution, the flux attenuation of the composite membrane F6 was relatively smaller than in the F0 membrane. This is mainly because the added O-MoS<sub>2</sub> increases hydrophilicity and negative charges to the composite membrane. Under stronger hydrophilicity and electrostatic repulsion, the adsorption capacity of the composite membrane surface to pollutants weakened, reducing the membrane flux decay rate after the solution concentration increased [45].

Three representative membranes, F0, F6, and F12, were selected for the interception flux test of different salt concentrations. Fig. 4g and h show the salt rejection rate and water flux for 1, 2, 3, 4, and 5 g/L Na<sub>2</sub>SO<sub>4</sub> solutions as a representative pollutant. In conclusion, the rejection rate of membranes at different concentrations was roughly F6 > F0 > F12. In

other words, when a specific amount of nanomaterials were added to the substrate matrix, the membrane performance would usher in an inflection point. However, it would deteriorate with the increase of nanomaterials. Besides, according to the Donnan balance, the ion concentration increase in the feed solution and weakens the Donnan repulsion between the fixed groups on the membrane surface and the ions of the same charge [46]. Therefore, the rejection performance of the membrane will decrease with the increase in salt concentration [47]. On the other hand, the increase in salt concentration had a greater impact on the rejection performance of F0 and F12, and the attenuation of rejection capacity was much greater than F6. This may be because the membrane pore morphology and size distribution of membrane F6 are superior to those of the other two membranes; it has better resistance to changes in feed and liquid conditions and better rejection performance [48]. On the other hand, with the concentration polarization effect, the water flux will also decrease with the increase of the feed liquid concentration. In the F6 and F12 membranes, with the better pore structure, the hydrophilicity of 2D nanoparticles and additional water channels provided by O-MoS<sub>2</sub> provided much greater water flux than the control membrane F0. However, in contrast, the water flux of membrane F6 is larger. Considering the changes in salt rejection performance, when the solution concentration reached 3 g/L, the salt rejection performance of the membrane appeared to decay significantly. However, the salt rejection rate gradually stabilized with further increased liquid feed concentration. In contrast, the membrane's water flux change did not change significantly with increasing feed concentration. Therefore, in combination with the change of water flux, a pressure of 4 bar and a salt concentration in a solution of 2 or 1 g/L, should be a more economical operating condition to maintain membrane performance.

To explore the impact of the chargeability of pollutant molecules on the membrane performance, three dye molecules with similar molecular weights but different charges, Jiana Green B (JGB), lemon yellow (LY), and CB (Table 3), were selected for interception and flux testing. The results are shown in Fig. 5a and b. The order of the rejection capacity (*R*) of dye molecules is  $R(\text{JGB}) > R(\text{LY}) > R(\text{CB})$ . The order of water flux ( $J_w$ ) follows the trend of  $J_w(\text{CB}) > J_w(\text{LY}) > J_w(\text{JGB})$ ,

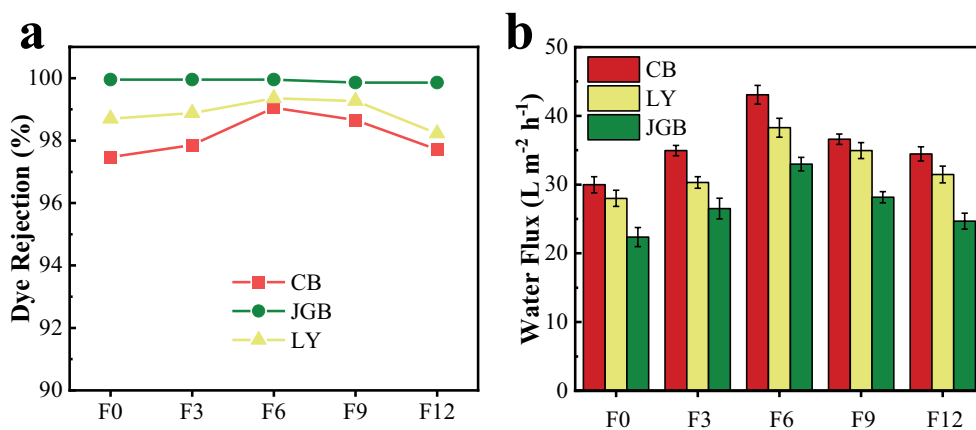


Fig. 5. Dye rejection flux diagram of different charges (a) dye rejection rate and (b) membrane flux diagram.



opposite of the rejection performance. This is because the pollutant molecules have different charges in the solution after hydrolysis. With the incorporation of nanoparticles and the negative charge of the NF membrane PA layer, the positively charged pollutant molecules in the water are adsorbed to the membrane surface due to electrostatic action. Then the membrane pores are blocked, rapidly forming a positively charged filter cake layer on the composite membrane's surface. Therefore, it is difficult for the remaining JGB molecules in the feed liquid to reach the surface of the composite membrane. This enhanced the rejection capacity of the membrane and greatly reduced the water flux of the membrane [44]. This is the trade-off effect of the membrane [49]. Among the membranes in the experiment, the modified membrane F6 stood out with a better decolorization rate, higher water flux, and less impact from changes in dye properties. In general, the charge changes of the pollutants had less effect on the modified membrane F6, mainly due to the smaller MWCO of the F6 membrane; therefore, the influence of the steric hindrance effect was greater when the dye molecules were retained.

### 3.2.2. Binary rejection performance test of dye and salt mixture

Since the actual dye wastewater is always a mixture of salt and dye, to explore the modified membrane's performance and treatment effect under actual conditions, 2 g/L sodium chloride and sodium sulfate were used as model

pollutants. Two different molecular weight dyes, RB and CB, were mixed at a concentration of 50 mg/L to simulate actual dye wastewater. The salt/dye rejection properties of the best-performing membrane F6 and the control membrane F0 were tested, and the results are shown in Fig. 6a and b. In general, the salt and dye blending will reduce the rejection of the membrane, especially salt rejection. The surface of the membrane adsorbs part of the hydrolyzed dye molecules through the charge effect, the electrostatic effect during the interception is weakened, and a part of the salt ions permeate the membrane [8]. Compared with the rejection results of a single salt solution, the rejection capacity of the actual wastewater was worse. Based on the same principle, the rejection of dye molecules by the membrane was also reduced. However, because the molecular size of the dye molecules used is larger than the pore size of the membrane and the salt ions; therefore, the interception mechanism of the two dyes was mainly a sieving effect; the electrostatic effect had only a minor contribution to it [50]. Meanwhile, the rejection performance of membrane F6 is much better for the two different membranes than that of the control membrane F0. Due to the pore structure optimization, under the influence of the mixed solution, the change of the salt and dye rejection performance of the hybrid membrane was smaller than the membrane F0. Especially in the rejection of dye, there was almost no change.

Fig. 6c and d show the membrane's rejection performance for salts and dyes in mixed solutions under different salt concentration conditions. For both membranes F0

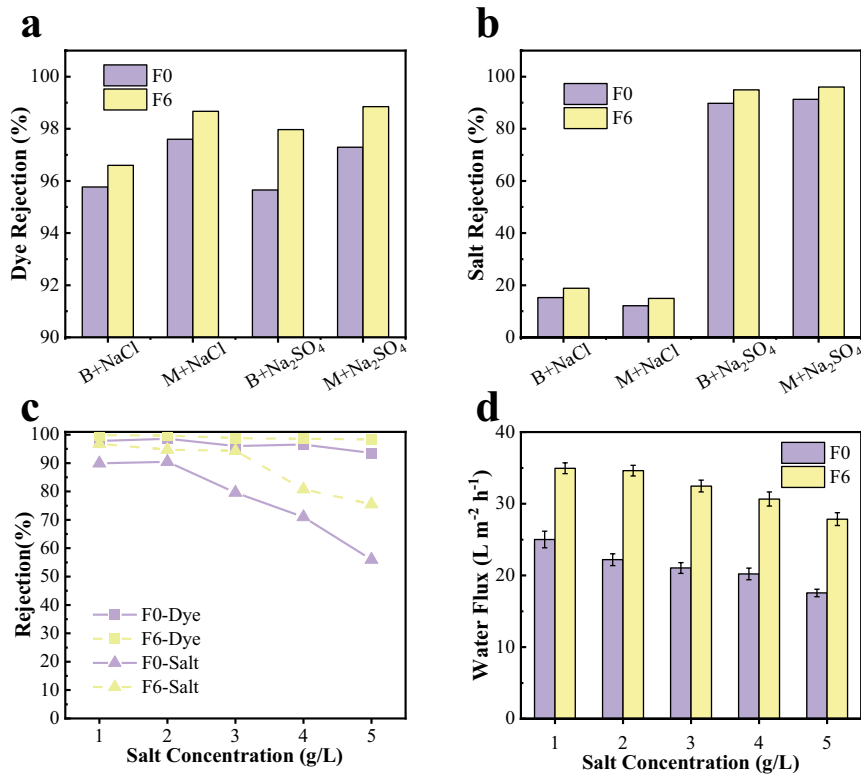


Fig. 6. Salt and dye mixed aqueous solution rejection and flux (a,b) salt retention in different mixed solutions, dye rejection, (c) different salt concentration on the rejection of salt and dye in the mixed solution, and (d) influence of total salt concentration in the mixed solution on flux.

and F6, salt concentration had little effect on dye rejection. Therefore, we choose to change the salt concentration to examine the dye/salt filtration performance of the NF membrane. In general, the higher the salt concentration in the liquid to be treated, the lower the salt removal efficiency of the membrane. This is the general retention law of NF membranes. At salt concentrations of 1–5 g/L, the filtration performance of the modified membrane F6 was better than the control membrane F0, and the attenuation rate of the membrane F6 (from 96.73% to 75.49%) was much lower than the F0 (from 89.92% to 55.99%). In addition to the electrostatic effect leading to saturation of the film surface charge, the addition of O-MoS<sub>2</sub> brings stronger stability to the modified substrate, enhances the mechanical strength of the film, and makes the film pores less susceptible to deformation and salt formation of the solution. When the wastewater's composition changes, the modified film's performance is more stable [51]; therefore, this base layer-modified composite NF membrane can be better applied to separation and filtration under complex conditions. Moreover, the rejection of control membrane F0 decayed faster with increasing salt concentration than membrane F6. In the modified membrane F6 the rejection changed significantly when the salt concentration reached 4 g/L due to the stronger electronegativity on the surface. In the range of 1–4 g/L Na<sub>2</sub>SO<sub>4</sub>, the modified membrane F6 maintained better performance and had a wider range of use conditions than the F0, but the F0 membrane showed a huge attenuation of rejection at 3 g/L [25]. Under this condition, there is little change in the performance of this guaranteed film (F6).

### 3.3. Flux stability test of the membrane

To investigate the dye desalination performance and flux change of the membrane, this experiment was equipped with 30 mg/L of RB and 2 g/L of Na<sub>2</sub>SO<sub>4</sub> mixed aqueous solution for a 120 h stability test. The water flux and rejection of the two membranes F0 and F6 during the operation period are shown in Fig. 7. Fig. 7a individually shows the water flux of the two membranes as a function of time. The membrane flux

slowly decreased during the filtration process, mainly due to the concentration polarization phenomenon and membrane surface pollution. Dye molecules and salt ions blocked the membrane pores, resulting in a decrease in water flux, and the adsorption on the membrane surface tends to balance [52]. In the same operation period, the water flux attenuation of the modified composite membrane F6 was significantly lower than the membrane F0. This means that the water flux of membrane F6 is relatively more stable, mainly because the membrane pores of the modified composite membrane are smaller, and the clogging degree of the membrane pores by dye molecules and salt ions will also be smaller. Explain from another angle, the 2D nanoparticles lightly improved the hydrophilicity and electronegativity of the NF membrane surface, enhanced the repulsion of the membrane to charged particles, and reduced the membrane water flux decay. On the other hand, the added 2D nanoparticles in the membrane substrate enhanced the composite membrane's mechanical strength, so the membrane maintained more stable physical properties under pressure. The strength and properties of the membrane pores also made the membrane water flux attenuation smaller [53].

Fig. 7b shows the changes in the salt and dye rejection rate for the two membranes during the 120 h operation. The Na<sub>2</sub>SO<sub>4</sub> rejection by the two membranes was above 95%, and the dye rejection was also above 99%. Overall, the salt and dye rejection of the modified composite membrane maintained a satisfactory result. As the running time increases, the rejection of salt and dye by the two membranes increases, opposite to the water flux change. This also can be explained by the phenomenon of concentration polarization and the contamination of the membrane by dye molecules, which weaken the water flux of the membrane while increasing its rejection performance when the pollutants block the membrane pores. During the long-term operation, the salt and dye rejection rates of the control membrane F0 showed pronounced changes, but the rejection performance was not stable [54]. This can be mainly attributed to the compaction effect of the membrane. Nevertheless, the modified membrane F6 effectively enhanced the membrane's

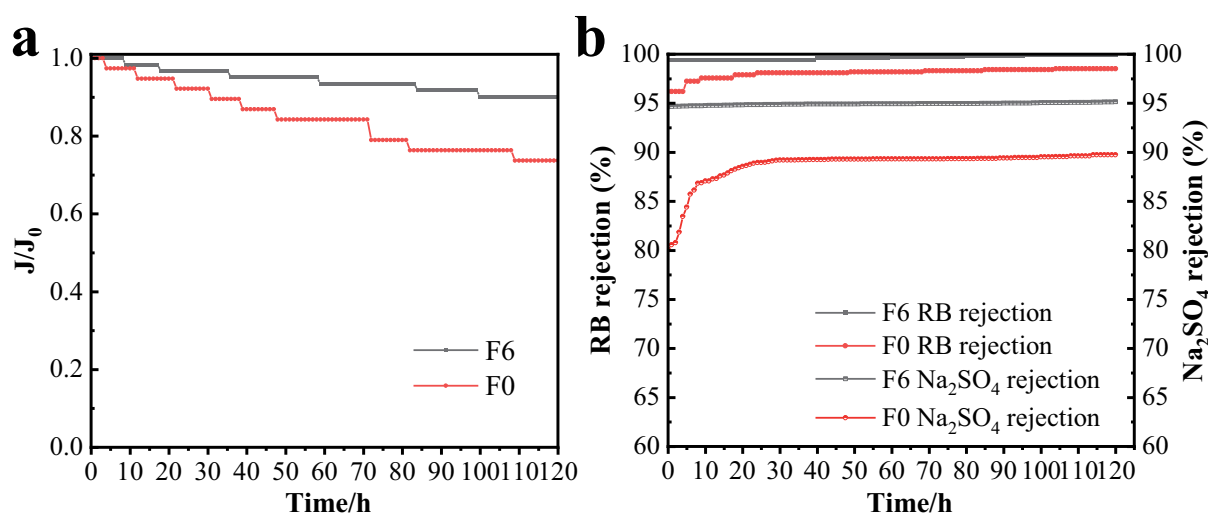


Fig. 7. Operating flux and rejection (a) flux normalization and (b) salt and dye rejection of F0 and F6 membrane.

Table 4  
Separation selectivity of various NF membranes for dye and NaCl rejection

Membrane	Feeds	Pressure (MPa)	Water flux (L/m <sup>2</sup> -h)	Rejection of salt (%)	Removal rate of dye (%)	Published year and Reference
O-MoS <sub>2</sub> -base/PSf	Chromotropic acid 2B/NaCl	0.4	30.15	18.83	96.6	This work
GO/NH <sub>2</sub> -Fe <sub>3</sub> O <sub>4</sub> /PVDF	Congo red/NaCl	0.5	~14.0	~15.00	>95.00	2020 [55]
PEA/TMC/PSf	Methyl blue/NaCl	0.4	17.75	17.8	95.03	2020 [56]
TiO <sub>2</sub> -COOH/CaAlg	Congo red/NaCl	0.4	14.1	9	95.5	2015 [57]
TiO <sub>2</sub> -polyarylate	Congo red/NaCl	0.4	20.5	5.2	96.3	2018 [58]
ZDNMA/TMC	MYB/NaCl	0.6	24.2	~10.7	91.9	2019 [59]
Catechin-chitosan/HPAN	Acid fuchsin/NaCl	0.4	7.2	12.5	98.7	2020 [60]

mechanical properties due to the addition of 2D nanoparticles in the membrane matrix, making the rejection performance of the membrane more stable. During the operation, the membrane F6 showed overall better performance.

The F6 membrane dye/salt separation performance was compared with the performance of other membranes reported in recent years. Table 4 presents specific information on various membranes' dye/salt separation. Among the membranes, our membrane had the highest water flux and showed superior performance in NaCl salt retention. Some membranes performed better for dye removal, but their water flux was much lower than the O-MoS<sub>2</sub>-based modified membrane used here. Therefore, our membranes have better overall performance.

#### 4. Conclusion

This work reports the results of using the O-MoS<sub>2</sub>-based membrane-modified NF membranes prepared in previous work to treat a variety of simulated wastewaters. The base membrane-modified NF membrane effectively improved the membrane's filtration performance. When treating dye-containing wastewater (CB and RB) for the best performing composite membrane F6, the water flux reached 43.73 and 43.24 L/m<sup>2</sup>-h, respectively. Compared to control membrane, the membrane F6 also exhibited excellent dye/salt selectivity. In contrast, the change in salt and dye rejection of the modified membrane was significantly smaller than the control membrane in the salt content range of 1–5 g/L. This indicates that this base-membrane modified NF membrane had a wider range of applications and a better ability to maintain performance against complex and variable wastewater conditions. Meanwhile, in the long-term stability test, the effect of compaction on membrane performance was reduced when the base-membrane modified nanofiltration membrane was operated under pressure during nanofiltration due to the improved mechanical properties of the membrane substrate. This base-membrane modified NF membrane has strong filtration performance and stability, has a broader range of use, and has little impact on membrane performance under changing and complex conditions. This reproducible and easy-to-fabricate NF membrane provides a broader prospect for practical wastewater treatment in the future.

#### Declaration of competing interest

There are no conflicts to declare.

#### Acknowledgements

This work was supported by grants from the Postdoctoral Science Foundation, the PhD Project (No. 2019-YYB-05) and Generalized System of Preferences – One Type Project (No. 2019-XTPH1-05) of Jiangxi Academy of Sciences, the key research and development – key project of Jiangxi Province, China (No. 20212BBG71001).

#### References

- [1] Y. Geng, B. Doberstein, Developing the circular economy in China: challenges and opportunities for achieving 'leapfrog development', *Int. J. Sustainable Dev. World Ecol.*, 15 (2008) 231–239.
- [2] J. Liang, X.-a. Ning, J. Sun, J. Song, J. Lu, H. Cai, Y. Hong, Toxicity evaluation of textile dyeing effluent and its possible relationship with chemical oxygen demand, *Ecotoxicol. Environ. Saf.*, 166 (2018) 56–62.
- [3] K. Balapure, K. Jain, N. Bhatt, D. Madamwar, Exploring bioremediation strategies to enhance the mineralization of textile industrial wastewater through sequential anaerobic-microaerophilic process, *Int. Biodeterior. Biodegrad.*, 106 (2016) 97–105.
- [4] L. Bilińska, M. Gmurek, S. Ledakowicz, Comparison between industrial and simulated textile wastewater treatment by AOPs – biodegradability, toxicity and cost assessment, *Chem. Eng. J.*, 306 (2016) 550–559.
- [5] W.-J. Lau, A.F. Ismail, Polymeric nanofiltration membranes for textile dye wastewater treatment: Preparation, performance evaluation, transport modelling, and fouling control – a review, *Desalination*, 245 (2009) 321–348.
- [6] H. Nawaz, M. Umar, I. Nawaz, A. Ullah, M. Tauseef Khawar, M. Nikiel, H. Razzaq, M. Siddiq, X. Liu, Hybrid PVDF/PANI membrane for removal of dyes from textile wastewater, *Adv. Eng. Mater.*, 24 (2022) 2100719, doi: 10.1002/adem.202100719.
- [7] K. Rambabu, G. Bharath, P. Monash, S. Velu, F. Banat, Mu. Naushad, G. Arthanareeswaran, P. Loke Show, Effective treatment of dye polluted wastewater using nanoporous CaCl<sub>2</sub> modified polyethersulfone membrane, *Process Saf. Environ. Prot.*, 124 (2019) 266–278.
- [8] T. Puspasari, K.-V. Peinemann, Application of thin film cellulose composite membrane for dye wastewater reuse, *J. Water Process Eng.*, 13 (2016) 176–182.
- [9] M. Kamali, D.P. Suhas, M.E. Costa, I. Capela, T.M. Aminabhavi, Sustainability considerations in membrane-based technologies for industrial effluents treatment, *Chem. Eng. J.*, 368 (2019) 474–494.
- [10] S.K. Nataraj, K.M. Hosamani, T.M. Aminabhavi, Nanofiltration and reverse osmosis thin film composite membrane module for the removal of dye and salts from the simulated mixtures, *Desalination*, 249 (2009) 12–17.
- [11] R. Weng, X. Huang, D. Liao, S. Xu, L. Peng, X. Liu, A novel cellulose/chitosan composite nanofiltration membrane

- prepared with piperazine and trimesoyl chloride by interfacial polymerization, *RSC Adv.*, 10 (2020) 1309–1318.
- [12] X. Feng, D. Peng, J. Zhu, Y. Wang, Y. Zhang, Recent advances of loose nanofiltration membranes for dye/salt separation, *Sep. Purif. Technol.*, 285 (2022) 120228, doi: 10.1016/j.seppur.2021.120228.
- [13] Y. Wang, Y. Ren, H. Wu, X. Wu, H. Yang, L. Yang, X. Wang, Y. Wu, Y. Liu, Z. Jiang, Amino-functionalized ZIF-7 embedded polymers of intrinsic microporosity membrane with enhanced selectivity for biogas upgrading, *J. Membr. Sci.*, 602 (2020) 117970, doi: 10.1016/j.memsci.2020.117970.
- [14] J.-J. Han, Q.-Y. Zhang, M.-Y. Huang, Y. Chen, X. Yan, W.-Z. Lang, Two-dimensional WS<sub>2</sub> membranes constructed on different substrates for efficient dye desalination, *Desalination*, 480 (2020) 114380, doi: 10.1016/j.desal.2020.114380.
- [15] Z. Zhang, G. Kang, H. Yu, Y. Jin, Y. Cao, From reverse osmosis to nanofiltration: precise control of the pore size and charge of polyamide membranes via interfacial polymerization, *Desalination*, 466 (2019) 16–23.
- [16] S. Yang, Q. Jiang, K. Zhang, Few-layers 2D O–MoS<sub>2</sub> TFN nanofiltration membranes for future desalination, *J. Membr. Sci.*, 604 (2020) 118052, doi: 10.1016/j.memsci.2020.118052.
- [17] Q. Jiang, H. Tian, K. Zhang, Enhanced performance of poly(M-phenylene isophthalamide) (PMIA) composite hollow fiber ultrafiltration membranes by O–MoS<sub>2</sub> nanosheets modification, *Desal. Water Treat.*, 166 (2019) 245–258.
- [18] S.H. Maruf, A.R. Greenberg, Y. Ding, Influence of substrate processing and interfacial polymerization conditions on the surface topography and permselective properties of surface-patterned thin-film composite membranes, *J. Membr. Sci.*, 512 (2016) 50–60.
- [19] N. Misdan, W.J. Lau, A.F. Ismail, T. Matsuura, D. Rana, Study on the thin film composite poly(piperazine-amide) nanofiltration membrane: impacts of physicochemical properties of substrate on interfacial polymerization formation, *Desalination*, 344 (2014) 198–205.
- [20] N. Misdan, W.J. Lau, A.F. Ismail, T. Matsuura, Formation of thin film composite nanofiltration membrane: effect of polysulfone substrate characteristics, *Desalination*, 329 (2013) 9–18.
- [21] T. Kamada, T. Ohara, T. Shintani, T. Tsuru, Controlled surface morphology of polyamide membranes via the addition of co-solvent for improved permeate flux, *J. Membr. Sci.*, 467 (2014) 303–312.
- [22] F.G. Donnan, Theory of membrane equilibria and membrane potentials in the presence of non-dialysing electrolytes. A contribution to physical-chemical physiology, *J. Membr. Sci.*, 100 (1995) 45–55.
- [23] G.S. Lai, W.J. Lau, P.S. Goh, A.F. Ismail, N. Yusof, Y.H. Tan, Graphene oxide incorporated thin film nanocomposite nanofiltration membrane for enhanced salt removal performance, *Desalination*, 387 (2016) 14–24.
- [24] J.-A.-D. Sharabati, S. Guclu, S. Erkoc-Ilter, D.Y. Koseoglu-Imer, S. Unal, Y.Z. Menceloglu, I. Ozturk, I. Koyuncu, Interfacially polymerized thin-film composite membranes: impact of support layer pore size on active layer polymerization and seawater desalination performance, *Sep. Purif. Technol.*, 212 (2019) 438–448.
- [25] J. Yu, Y. Zhang, J. Chen, L. Cui, W. Jing, Solvothermal-induced assembly of 2D-2D rGO-TiO<sub>2</sub> nanocomposite for the construction of nanochannel membrane, *J. Membr. Sci.*, 600 (2020) 117870, doi: 10.1016/j.memsci.2020.117870.
- [26] X. Wang, Q. Xiao, C. Wu, P. Li, S. Xia, Fabrication of nanofiltration membrane on MoS<sub>2</sub> modified PVDF substrate for excellent permeability, salt rejection, and structural stability, *Chem. Eng. J.*, 416 (2021) 129154, doi: 10.1016/j.cej.2021.129154.
- [27] H. Gao, Q. Shi, D. Rao, Y. Zhang, J. Su, Y. Liu, Y. Wang, K. Deng, R. Lu, Rational design and strain engineering of nanoporous boron nitride nanosheet membranes for water desalination, *J. Phys. Chem. C*, 121 (2017) 22105–22113.
- [28] R. Zhang, S. Yu, W. Shi, W. Wang, X. Wang, Z. Zhang, L. Li, B. Zhang, X. Bao, A novel polyestaramide thin film composite nanofiltration membrane prepared by interfacial polymerization of serinol and trimesoyl chloride (TMC) catalyzed by 4-dimethylaminopyridine (DMAP), *J. Membr. Sci.*, 542 (2017) 68–80.
- [29] R. Zhang, S. Yu, W. Shi, J. Zhu, B. Van der Bruggen, Support membrane pore blockage (SMPB): an important phenomenon during the fabrication of thin film composite membrane via interfacial polymerization, *Sep. Purif. Technol.*, 215 (2019) 670–680.
- [30] J. Ji, R.F. Childs, M. Mehta, Mathematical model for encapsulation by interfacial polymerization, *J. Membr. Sci.*, 192 (2001) 55–70.
- [31] F. Zhang, J.-b. Fan, S. Wang, Interfacial polymerization: from chemistry to functional materials, *Angew. Chem. Int. Ed.*, 59 (2020) 21840–21856.
- [32] J. Hwan Mo, Y. Hwan Lee, J. Kim, J. Yun Jeong, J. Jegal, Treatment of dye aqueous solutions using nanofiltration polyamide composite membranes for the dye wastewater reuse, *Dyes Pigm.*, 76 (2008) 429–434.
- [33] J. Zhang, Z. Li, K. Zhan, R. Sun, Z. Sheng, M. Wang, S. Wang, X. Hou, Two dimensional nanomaterial-based separation membranes, *Electrophoresis*, 40 (2019) 2029–2040.
- [34] T.D. Matthews, H. Yan, D.G. Cahill, O. Coronell, B.J. Mariñas, Growth dynamics of interfacially polymerized polyamide layers by diffuse reflectance spectroscopy and Rutherford backscattering spectrometry, *J. Membr. Sci.*, 429 (2013) 71–80.
- [35] A.K. Ghosh, E.M.V. Hoek, Impacts of support membrane structure and chemistry on polyamide–polysulfone interfacial composite membranes, *J. Membr. Sci.*, 336 (2009) 140–148.
- [36] F. Liu, L.L. Wang, D. Li, Q. Liu, B. Deng, A review: the effect of the microporous support during interfacial polymerization on the morphology and performances of a thin film composite membrane for liquid purification, *RSC Adv.*, 9 (2019) 35417–35428.
- [37] X. Kang, Y. Cheng, Y. Wen, J. Qi, X. Li, Bio-inspired co-deposited preparation of GO composite loose nanofiltration membrane for dye contaminated wastewater sustainable treatment, *J. Hazard. Mater.*, 400 (2020) 123121, doi: 10.1016/j.jhazmat.2020.123121.
- [38] W. Yan, Z. Wang, J. Wu, S. Zhao, J. Wang, S. Wang, Enhancing the flux of brackish water TFC RO membrane by improving support surface porosity via a secondary pore-forming method, *J. Membr. Sci.*, 498 (2016) 227–241.
- [39] W.-J. Lau, G.-S. Lai, J. Li, S. Gray, Y. Hu, N. Misdan, P.-S. Goh, T. Matsuura, I.W. Azelee, A.F. Ismail, Development of microporous substrates of polyamide thin film composite membranes for pressure-driven and osmotically-driven membrane processes: a review, *J. Ind. Eng. Chem.*, 77 (2019) 25–59.
- [40] W. Ye, J. Lin, R. Borrego, D. Chen, A. Sotto, P. Luis, M. Liu, S. Zhao, C.Y. Tang, B. Van der Bruggen, Advanced desalination of dye/NaCl mixtures by a loose nanofiltration membrane for digital ink-jet printing, *Sep. Purif. Technol.*, 197 (2018) 27–35.
- [41] C.Y. Tang, T.H. Chong, A.G. Fane, Colloidal interactions and fouling of NF and RO membranes: a review, *Adv. Colloid Interface Sci.*, 164 (2011) 126–143.
- [42] X.Q. Gao, K.C. Yu, X.M. Wang, Rejection behaviors and separation selectivity of loose nanofiltration membranes for mineral ions in drinking water, *Huanjing Kexue Xuebao/Acta Sci. Circum.*, 40 (2020) 2700–2707.
- [43] P. Lu, S. Liang, L. Qiu, Y. Gao, Q. Wang, Thin film nanocomposite forward osmosis membranes based on layered double hydroxide nanoparticles blended substrates, *J. Membr. Sci.*, 504 (2016) 196–205.
- [44] E.M.V. Hoek, M. Elimelech, Cake-enhanced concentration polarization: a new fouling mechanism for salt-rejecting membranes, *Environ. Sci. Technol.*, 37 (2003) 5581–5588.
- [45] G.-R. Xu, J.-M. Xu, H.-J. Feng, H.-L. Zhao, S.-B. Wu, Tailoring structures and performance of polyamide thin film composite (PA-TFC) desalination membranes via sublayers adjustment—a review, *Desalination*, 417 (2017) 19–35.
- [46] S. Tul Muntha, A. Kausar, M. Siddiq, Advances in polymeric nanofiltration membrane: a review, *Polym. Plast. Technol. Eng.*, 56 (2017) 841–856.
- [47] H. Al-Zoubi, W. Omar, Rejection of salt mixtures from high saline by nanofiltration membranes, *Korean J. Chem. Eng.*, 26 (2009) 799–805.

- [48] J. Li, M. Wei, Y. Wang, Substrate matters: the influences of substrate layers on the performances of thin-film composite reverse osmosis membranes, *Chin. J. Chem. Eng.*, 25 (2017) 1676–1684.
- [49] H.B. Park, J. Kamcev, L.M. Robeson, M. Elimelech, B.D. Freeman, Maximizing the right stuff: the trade-off between membrane permeability and selectivity, *Science*, 356 (2017) 1138–1148.
- [50] T. Tavangar, K. Jalali, M.A. Alaei Shahmirzadi, M. Karimi, Toward real textile wastewater treatment: membrane fouling control and effective fractionation of dyes/inorganic salts using a hybrid electrocoagulation – nanofiltration process, *Sep. Purif. Technol.*, 216 (2019) 115–125.
- [51] S. Yang, H. Tian, M.R. Hill, K. Zhang, Effect and regulation mechanism of oxidation degrees on the O–MoS<sub>2</sub> structure and separation performance of nanofiltration membrane, *J. Membr. Sci.*, 635 (2021) 119468, doi: 10.1016/j.memsci.2021.119468.
- [52] S. Samsami, M. Mohamadizani, M.-H. Sarrafzadeh, E.R. Rene, M. Firoozbahr, Recent advances in the treatment of dye-containing wastewater from textile industries: overview and perspectives, *Process Saf. Environ. Prot.*, 143 (2020) 138–163.
- [53] G.-R. Xu, J.-M. Xu, H.-C. Su, X.-Y. Liu, Lu-Li, H.-L. Zhao, H.-J. Feng, R. Das, Two-dimensional (2D) nanoporous membranes with sub-nanopores in reverse osmosis desalination: latest developments and future directions, *Desalination*, 451 (2019) 18–34.
- [54] Q. Zhang, L. Fan, Z. Yang, R. Zhang, Y.-n. Liu, M. He, Y. Su, Z. Jiang, Loose nanofiltration membrane for dye/salt separation through interfacial polymerization with *in-situ* generated TiO<sub>2</sub> nanoparticles, *Appl. Surf. Sci.*, 410 (2017) 494–504.
- [55] L. Dong, M. Li, S. Zhang, X. Si, Y. Bai, C. Zhang, NH<sub>2</sub>-Fe<sub>3</sub>O<sub>4</sub>-regulated graphene oxide membranes with well-defined laminar nanochannels for desalination of dye solutions, *Desalination*, 476 (2020) 114227, doi: 10.1016/j.desal.2019.114227.
- [56] Y.F. Mi, N. Wang, Q. Qi, B. Yu, X.D. Peng, Z.H. Cao, A loose polyamide nanofiltration membrane prepared by polyether amine interfacial polymerization for dye desalination, *Sep. Purif. Technol.*, 248 (2020) 117079, doi: 10.1016/j.seppur.2020.117079.
- [57] Z. Qiao, Z. Wang, C. Zhang, S. Yuan, Y. Zhu, J. Wang, S. Wang, PVAm-PIP/PS composite membrane with high performance for CO<sub>2</sub>/N<sub>2</sub> separation, *AIChE J.*, 59 (2012) 215–228.
- [58] S. Chen, Y. Xie, T. Xiao, W. Zhao, J. Li, C. Zhao, Tannic acid-inspiration and post-crosslinking of zwitterionic polymer as a universal approach towards antifouling surface, *Chem. Eng. J.*, 337 (2018) 122–132.
- [59] Y.-F. Mi, G. Xu, Y.-S. Guo, B. Wu, Q.-F. An, Development of antifouling nanofiltration membrane with zwitterionic functionalized monomer for efficient dye/salt selective separation, *J. Membr. Sci.*, 601 (2020) 117795, doi: 10.1016/j.memsci.2019.117795.
- [60] Q. Long, Z. Zhang, G. Qi, Z. Wang, Y. Chen, Z.Q. Liu, Fabrication of chitosan nanofiltration membranes by the film casting strategy for effective removal of dyes/salts in textile wastewater, *ACS Sustainable Chem. Eng.*, 8 (2020) 2512–2522.

### Supporting information

In order to test the pore size and pore size distribution of the membrane, the pore size and pore size distribution of the membrane were obtained by calculating the rejection rate of polyethylene glycol (PEG) molecules with different molecular weights at 1,000 ppm concentration at 25°C and corresponding pressure conditions. The 90% rejection corresponds to the molecular weight cut-off of the membrane and the 50% rejection corresponds to the mean effective membrane pore size ( $\mu\text{P}$ ). Membrane pore size and pore size distribution were calculated using Eq. (S1)–(S3), as previously reported.

$$a = 16.73 \times 10^{-10} \times M_{\text{PEG}}^{0.557} \quad (\text{S1})$$

$$d_s = 2 \times a \times 10^7 \quad (\text{S2})$$

Table S1

Casting fluid viscosity data (mPa·s)

Rotating speed (r/min)	F0	F3	F6	F9	F12
700	258	265	276	278	287
900	256.7	258.9	265.8	274.2	285.8

$$\frac{dR(d_p)}{dd_p} = \frac{1}{d_p \ln \sigma_p \sqrt{2\pi}} \exp \left[ -\frac{(\ln d_p - \ln \mu_p)^2}{2(\ln \sigma_p)^2} \right] \quad (\text{S3})$$

where  $a$  (cm) and  $d_s$  (nm) are the Stokes radius and diameter of PEG, respectively. In general, when PEG rejection reaches 50%, the resulting  $d_s$  value ( $\mu\text{S}$ ) is approximately expressed as the average effective pore size ( $\mu\text{P}$ ) of the membrane.

Table S2

Surface roughness parameters of the modified membranes with different loading content of O-MoS<sub>2</sub>

Membrane no.	$R_a$ (nm)	$R_q$ (nm)	$R_z$ (nm)
F0	15.7	21.3	44.8
F3	18.2	26.3	61.4
F6	18.4	23.4	24.8
F9	18.8	24.1	65.2
F12	19.4	24.9	49.4